nature materials

ARTICLES

PUBLISHED ONLINE: 20 MARCH 2011 | DOI: 10.1038/NMAT2982

Memory and topological frustration in nematic liquid crystals confined in porous materials

Takeaki Araki[1,2], Marco Buscaglia[3], Tommaso Bellini[3]* and Hajime Tanaka[1]*

Orientational ordering is key to functional materials with switching capability, such as nematic liquid crystals and ferromagnetic and ferroelectric materials. We explored the confinement of nematic liquid crystals in bicontinuous porous structures with smooth surfaces that locally impose normal orientational order on the liquid crystal. We find that frustration leads to a high density of topological defect lines permeating the porous structures, and that most defect lines are made stable by looping around solid portions of the confining material. Because many defect trajectories are possible, these systems are highly metastable and efficient in memorizing the alignment forced by external fields. Such memory effects have their origin in the topology of the confining surface and are maximized in a simple periodic bicontinuous cubic structure. We also show that nematic liquid crystals in random porous networks exhibit a disorder-induced slowing-down typical of glasses that originates from activated collisions and rearrangements of defect lines. Our findings offer the possibility to functionalize orientationally ordered materials through topological confinement.

Materials exhibiting spontaneous orientational order, such as nematic liquid crystals (NLCs) and ferromagnetic and ferroelectric materials, have tremendous impact on our lifestyle because of their switching capability under an external field. The growing interest in integration of these ordered materials in devices based on heterogeneous micro- and nanostructures brings about the need to understand the effects of confinement and interface coupling on their spontaneous ordering. Because of its soft ordering and liquid nature, the NLC phase is an ideal system to study the effects of such incorporation in heterogeneous structures and to investigate if and how this may lead to new material properties[1–3]. When an NLC is confined in a solid porous medium, coupling of the molecular symmetry axis (the director) to the solid surface may easily conflict with the symmetry of the ordered phase and thus lead to frustration and topological defects. For example, NLCs cannot match, without point defects or disclination lines (DLs), the constraint of normal alignment on spherical surfaces, either when enclosed in a spherical cavity or when hosting spherical particles[2,4–9]. A number of studies have been devoted to phase behaviour and optical properties of NLCs confined in a variety of structures[2]. Various properties emerging from confinement have been reported, including previously unknown phase transitions, extreme optical turbidity and glassy behaviour. Specifically, non-ergodicity and slow dynamics have been found by studying NLCs perturbed by the random nanostructures of silica gels[10–13], and in NLCs incorporated in microstructured porous networks with smooth surfaces such as polymer filters and compacted colloidal spheres[14,15]. Interpretation of the glassy dynamics of these systems has been given in the frame of 'random-field' Ising-type models[13,16–18], in which point-like disorder forces the local NLC orientation and pins topological defect lines. This interpretation cannot be applied to most of the confining geometries, nor does it enable material design. We provide here a more general framework for the origin of non-ergodicity in confined NLCs, based on the smooth surface field provided by the connected geometry of porous networks with no need for distributed point-like pinning sites. Specifically, we report a computer simulation study of NLCs in bicontinuous confining structures. The choice of bicontinuity stems from practical considerations because this property is necessary to design robust host structures in which to insert NLCs by flow. We have considered porous structures with smooth surfaces that provide anchoring of the NLC orientation normal to the surfaces and thus promote local ordering. We always find that on confinement the NLC develops strong non-ergodic behaviour and memory effects, and we demonstrate this to be a property intrinsic to the basic topology of the confining surfaces, with no need for randomness. Moreover, we show that the topology of the pores, which controls the number of disclination defect lines through curvature, determines the amount of order that can be permanently written in the system by external fields. Accordingly, we propose a simple periodic structure that maximizes the memory capability of the system. These results offer new possibilities for material functionalization by geometrical confinement in suitably designed porous media. Given the growing capacity for three-dimensional microfabrication, these concepts could guide the design of new materials for electro-optical applications.

We have carried out lattice-based Monte Carlo simulations in which headless spins interacting through the Lebwohl–Lasher potential are confined into four topologically distinct porous structures with locally smooth surfaces and perpendicular nematic anchoring, as shown in Fig. 1 (see Methods). We considered one random porous matrix structure (RPM) and three regular bicontinuous ordered porous structures: one bicontinuous cubic (BC) (see also Fig. 2), one simple cubic packing of connected (mutually touching) spheres (SC_c) and one cubic network of cylindrical holes (Cyl). To assess the importance of the bicontinuous nature of the structures, we also studied a simple cubic array of spheres that are not in contact (SC_n). The RPM and SC are thought to mimic systems that have been already considered experimentally: NLCs in Millipore filtering membranes[12,14] and NLCs in the interstitial spaces of a hard-sphere colloidal crystal[15]. We have studied NLCs

[1]Institute of Industrial Science, University of Tokyo, 4-6-1 Komaba, Meguro-ku, Tokyo 153-8505, Japan, [2]Department of Physics, Kyoto University, Kitashirakawa-Oiwakecho, Sakyo-ku, Kyoto 606-8502, Japan, [3]Dipartimento di Chimica, Biochimica e Biotecnologie per la Medicina, Università di Milano, Via F.lli Cervi 93, 20090 Segrate (MI), Italy. *e-mail: tommaso.bellini@unimi.it; tanaka@iis.u-tokyo.ac.jp.

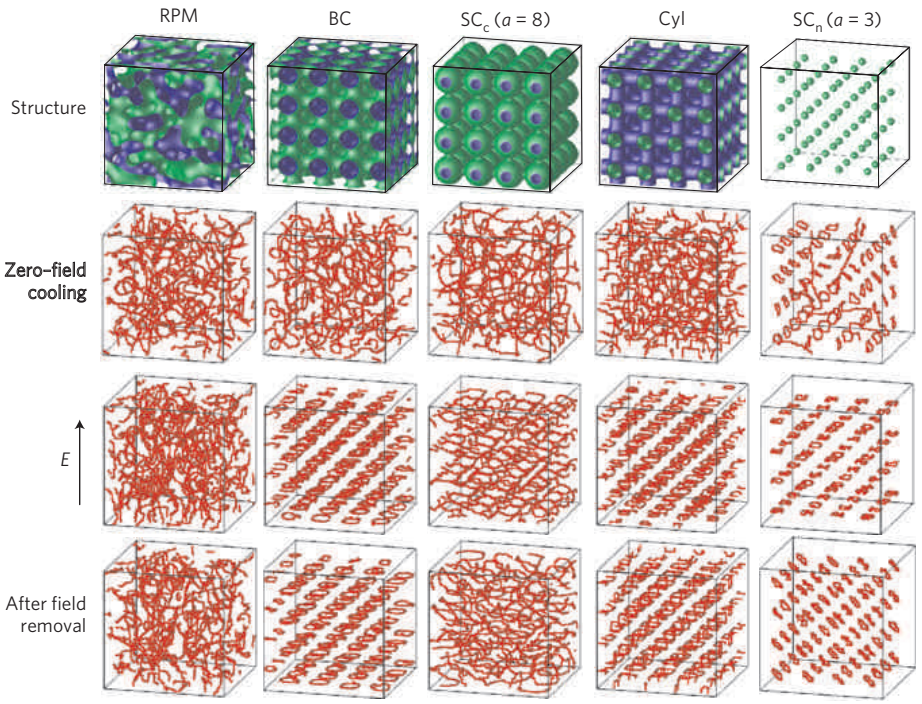

Figure 1 | Patterns of DLs in porous media with various topologies. Top row: porous structures considered in this article. The structures are shown in blue and green (blue for the interior and green for the surface in contact with NLCs). Left to right: Random porous media (RPM), bicontinuous cubic (BC), simple cubic packing of connected spheres (SC_c), three-dimensional array of cylindrical channels (Cyl) and simple cubic array of non-contacting isolated spheres (SC_n). In SC_c, each sphere contacts the six nearest spheres, so that the porous matrix forms a continuous structure. In SC_n, on the other hand, the spheres are isolated. Second row: DLs as obtained before the application of the field. Third row: DLs under a strong field ($E = 0.5$) along z axis, the direction indicated by the arrow. Bottom row: DLs remaining after removing the field. The simulation cubes are 64^3 and the lattice constants are $L = 16$ for periodical matrices. The radii a of spheres in SC_c and SC_n, and cylinders in Cyl, are 8, 3 and 4, respectively. See Supplementary Information for the scaling of variables.

incorporated in these structures as a function of the reduced temperature T and of the strength E of an external field (for the scaling of these and other variables, see Supplementary Information).

Memory effects have been found in all the explored systems, analogously to what is described in Fig. 2 for the case of BC (see also the Supplementary Information, for the case of RPM). We prepare the initial state by cooling the system to below the isotropic–nematic transition temperature T_{IN} and letting it equilibrate with no field applied ('zero-field cooling'). Zero-field-cooled states are locally ordered because their local nematic order parameter, a quantity expressing the amount of orientational order of neighbouring spins, is approximately equal to Q_B, the order parameter of the bulk material at the same temperature (see Methods for the definition of Q). At the same time, the systems are globally isotropic, and hence the nematic order parameter averaged on the whole sample is $Q = 0$. On these disordered stable states we apply an electric-field (E) pulse for a certain duration, and then switch it off. Time t is here represented by the number of Monte Carlo cycles (MCC). When the electric field is applied, the director is forced to be uniform. For the strongest field, $Q \approx Q_B$. On removing the field, the system relaxes to a metastable state with intermediate order, characterized by a remnant order Q_M (see Fig. 2a), a clear indication that the system has somehow memorized the field-induced order. The field-strength dependence of both Q_E—the order parameter in the presence of the field—and Q_M is shown in Fig. 2b for the case of BC. The memorization capability of the system crucially depends on the frustration imposed by the solid interfaces on the soft orientational ordering of NLCs. This is testified by the large number of topological defects, the DLs produced by the incompatibility of the anchoring constraints with the nematic ordering. We have located DLs inside the nematic domain ($\mathcal{N}$) according to ref. 19, and their trajectories are shown as red lines in Figs 1 and 2e. Many DLs are found wandering through the pores of all structures even after long annealing, in all three conditions here explored: after zero-field cooling (panels in the second row of Fig. 1), while the field is applied (third row of Fig. 1) and after the removal of the field (bottom row of Figs 1 and 2e).

Obviously, frustration imposed by surface anchoring plays a crucial role in the above behaviour. The enormously large number of possible topological states of the confined NLC (see Supplementary Information) suggests an apparent analogy to well-known frustrated systems, spin and structural glass, in which an exponentially large number of metastable states are separated by large barriers. The origin of frustration is, however, quite different in the two systems. Typical spin glasses are intrinsically frustrated because of the impossibility to simultaneously minimize all coupling energies. In the case of confined nematics, confinement and topology provide frustration to an otherwise well-behaved system. While locally the nematic order is well defined, on the length scale of the pores the behaviour of the system becomes frustrated and metastable because of the impossibility to simultaneously match all the anchoring constraints without topological defects. This induced frustration offers the possibility to design confining geometries that optimize the macroscopic (for example, optical) properties of the metastable states through 'geometrical functionalization' of materials.

Inspection of the defect trajectories indicates that in all geometries the onset of remnant order is associated with a change in the way DL loops are concatenated to the solid matrix. In the case of a weak field, such as the weakest field in Fig. 2a, DLs respond just elastically to the field (no change in their topology) and, on removing the field, DLs relax back to their original trajectories. On the other hand, application of stronger external

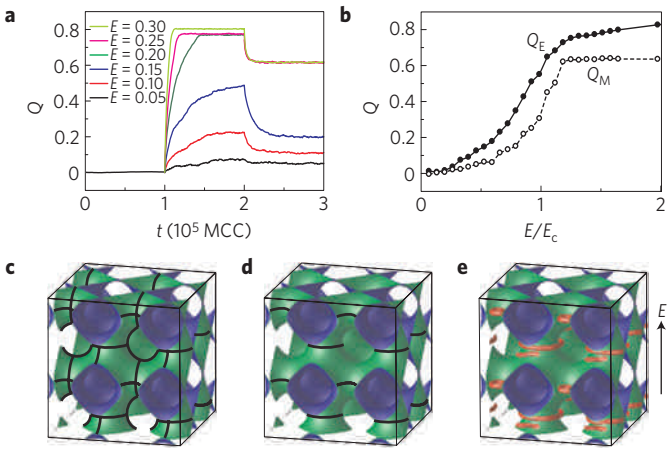

Figure 2 | Memory effects in NLCs confined in a bicontinuous cubic porous medium (BC). a, Computer-simulated evolutions of the nematic order parameter Q of an NLC incorporated into a BC ($L = 32$) as the field is first applied (at $t = 10^5$ MCC) and later removed (at $t = 2 \times 10^5$ MCC) for various choices of field strength, ranging from weak ($E = 0.05$, black) to strong ($E = 0.3$, light green). **b**, Nematic order parameters Q_E (filled symbols) and Q_M (open symbols), extracted from the simulations in **a**, as a function of the field strength E normalized by the threshold value E_c (=0.152). **c**,**d**, Snapshots of BC, where we mark by black lines the loci of largest negative Gaussian curvature (**c**) and the location where the surface is normal to the z-axis, which is indicated by the arrow (**d**). **e**, DLs (red lines) remaining after switching off a strong field ($E = 1.0$) along z.

fields supplies enough energy to reconfigure the DL trajectories, producing different closed loops through the connective paths of $\mathcal{N}$. In the limit of very strong fields, DLs are forced against surface regions for which the normal lies in the x–y plane. The application of a strong field may even break the anchoring (more details in Supplementary Information). However, as the field is removed, the normal anchoring is recovered and DLs relax to the local elastic energy minimum while preserving in large part the concatenation with the solid network forced by the field, thus keeping some memory of the field effect. This leaves the system in a new aligned stable state with respect to the zero-field-cooled disordered stable state. In the absence of fields, elastic minimization is obtained when DLs run along lines of largest negative Gaussian curvature of the surface. These observations enable us to define criteria to maximize memory. Maximum memory is expected in systems where the DL paths forced by the field are best maintained after the field removal, while at the same time granting a large number of metastable states. Accordingly, we looked for a bicontinuous structure in which the loci of most negative Gaussian curvature would form loops lying on planes perpendicular to the external field. This is how we came to the BC structure, in which the locations where the surface has a normal in the x–y plane (Fig. 2d) are also locations of largest negative Gaussian curvature (Fig. 2c). The geometrical coincidence also holds after the field is removed, and thus the DL loops remain where they were forced by the field, as shown in Fig. 2e (more details in the Supplementary Information). Furthermore, the cubic symmetry of BC enables memorization in orthogonal directions, should the electrode design allow multiple field directions.

The topology-based non-ergodicity described here relies on the large energy necessary to 'reconfigure' irreducible DL loops, that is, to disconnect and reconnect them around a different choice of handles within the porous media. Bicontinuity is essential to this form of multistability. This can be appreciated by studying the behaviour of DLs in an array of isolated spheres (for example, SC_n). As expected, DLs compensate for the topological charge introduced by the homeotropically (radially, in this case) alignment-inducing spheres. As the equilibration proceeds, DLs anneal into 'Saturn rings'[5], one for each sphere. As the field is applied, the rings align (see Fig. 1). On field removal, rings can rotate around the spheres without topological changes. Saturn rings are held parallel to one another by mutual elastic interactions[7], and their collective rotation is nearly a soft mode of the SC_n structure. Accordingly, we find that, on turning off the field, the nematic order starts rotating at finite temperatures (see Fig. 2). In the same vein, we have observed that weak external fields are effective in reorienting the director (see Supplementary Information). In contrast, switching the alignment of NLCs in bicontinuous porous structures requires much larger values of E, indicating the presence of large energy barriers separating configurations with different topologies. We evaluate the energy required to induce a topological change in a bicontinuous structure as being of the order of 100 times larger than that necessary for reorienting the director in the SC_n system, which is of the order of $k_B T$.

NLCs in porous media relax differently depending on the geometry and topology. Figure 3a,b compares the pore-size (ℓ) dependence of the memorization effects of NLCs in RPM and BC at constant $T = 0.1$. The relaxations found after the removal of a strong field $E = 1$ are markedly different in the two systems (see also Supplementary Information). Relaxations of NLC order in the BC are characterized by a single decay process very well fitted by a stretched exponential

$$Q(t) = Q_M + \Delta Q_S \exp(-(t/\tau_S)^{\alpha}) \qquad (1)$$

where Q_M is the remnant order, determined as the long-time asymptote of $Q(t)$, and ΔQ_S is the amplitude of the stretched exponential. In the case of RPM, the decays do not saturate as clearly as in the case of BC, the first relaxation being followed by a very slow decay to a second plateau. We find the curves to be well fitted by a summation of two decay processes,

$$Q(t) = Q_M + \Delta Q_S e^{-(t/\tau_S)^{\alpha}} + \frac{\Delta Q_L}{1 + \log(1 + t/\tau_L)} \qquad (2)$$

where ΔQ_S and ΔQ_L are, respectively, the amplitudes of the fast stretched-exponential relaxation and of the slow decay. The slow decay could also be fitted by a stretched exponential but it seems to be better compatible with the functional shape in equation (2), chosen to cross over from a Lorentzian decay at small t to a logarithmic decay for $t > \tau_L$ (more details in Supplementary Information). In Fig. 3, fitted curves are drawn as black dashed lines in the background of the coloured lines showing the simulation results.

The parameters τ_S and α of the stretched exponential decay for both pore geometries are shown in Fig. 4a. The values obtained in the two geometries match, indicating that the fast decay is a relaxation process of general relevance. τ_S grows as ℓ^2 (dashed line), a scaling generally found for the viscoelastic relaxation of nematics in conventional liquid crystal cells (see Supplementary Information). Indeed, in these systems viscoelastic relaxation is expected to govern the evolution of the system from the field-induced ordered state to the configuration of minimum elastic energy attainable with no topological rearrangement. In the case of BC, such a configuration is characterized by DLs stabilized by the surface geometry, so that no further relaxation is observed at all ℓ values (Fig. 4b, open red dots). When instead the topology attained after the fast relaxation is not stabilized by surface design, rearrangements of DLs leading to a state with a lower energy are possible through a further slower relaxation, as observed in RPM. In this case Q_M is found to depend on ℓ (see Fig. 4b): on increasing ℓ, Q_M grows while ΔQ_L vanishes, so

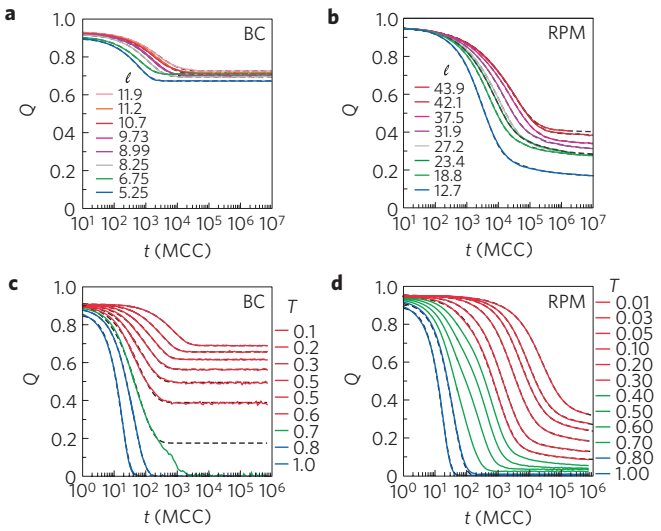

Figure 3 | Relaxation of the nematic order Q after turning off the field. **a**–**d**, Decay of Q at $T = 0.1$ for various pore sizes ℓ in BC (**a**) and RPM (**b**), and at fixed ℓ (BC: $\ell = 6.75$, RPM: $\ell = 12.7$) for various temperatures T in BC (**c**) and RPM (**d**). In all cases, $E = 1$. All simulation data are fitted as described in the text, and fitting curves are plotted as dashed black lines in the background. They are difficult to visualize because of the high quality of the fit. In **c** and **d** line colours indicate the various decay regimes. Blue, compressed exponential decay ($T > T_{IN}$); red, stretched exponential decay (BC) or decay in equation (2) (RPM) ($T < T_{IN}$); green, intermediate region where the combined decays are found.

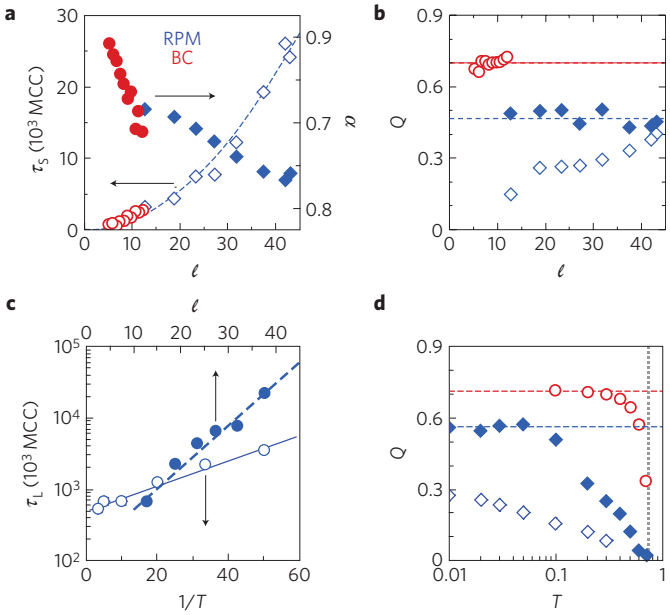

Figure 4 | ℓ and T dependencies of the parameters characterizing the order-parameter relaxation. **a**, ℓ dependence of τ_S and α of the stretched exponential decay for BC (red circles) and RPM (blue diamonds). The dashed line is a parabolic fit to the τ_S data (open symbols). **b**, ℓ dependence of the remnant order as expressed in BC by Q_M (open red circles), and in RPM by Q_M (open blue diamonds) and $Q_M + \Delta Q_L$ (filled blue diamonds). Lines indicate the remnant order expected in the limit of large ℓ. **c**, ℓ and $1/T$ dependence of the characteristic time of the logarithmic decay, τ_L. Lines represent the fitted activated behaviour $\tau_L = 135\exp(0.13\ell)$ (thick dashed line) and $\tau_L = 502\exp(0.041/T)$ (solid line). **d**, T dependence of the remnant order as expressed in BC by Q_M (open red circles), and in RPM by Q_M (open blue diamonds) and $Q_M + \Delta Q_L$ (filled blue diamonds). Horizontal dashed lines indicate the remnant order expected in the limit of low T. The vertical dotted line indicates the location of T_{IN}.

the quantity $Q_M + \Delta Q_L$ is independent of ℓ. Hence, in RPM, the NLC viscoelastically relaxes to a state that is independent of pore size and that can further relax only when the pores are small enough.

Figure 4c (top axis) shows the ℓ dependence of τ_L. τ_L seems to grow exponentially with ℓ, an indication that the slow relaxation results from an activated process, the energy-barrier scaling with ℓ (see Supplementary Information). A confirmation of this view is provided by the temperature dependence of $Q(t)$. In Fig. 3c,d we show the relaxation of the remnant nematic order following the removal of a strong field $E = 1$ at various T, respectively, for BC and RPM for a given ℓ. For both geometries, $Q(t)$ has a high-T regime (blue lines), featuring a single-compressed-exponential decay, a low-T regime (red lines), well described by equations (1) (BC) and (2) (RPM), and an intermediate regime (green lines), where a combination of elements is found (more details in Supplementary Information). The T dependence of Q_M is shown in Fig. 4d. In the case of BC, on lowering T, Q_M increases and reaches a plateau value at $T \approx 0.4$. In the case of RPM, instead, Q_M does not reach a T-independent value at low T. However, the quantity $Q_M + \Delta Q_L$ (solid blue diamonds) grows and saturates at $T \approx 0.1$, indicating that this temperature is below that at which viscoelastic decay takes place without rearrangement in the topology of DLs. In this low-T regime, the slow decay depends exponentially on T^{-1} (see Fig. 4c), again supporting the notion of an activated process underlying the slow decay. This picture is also confirmed by the shape of the slow relaxations, because logarithmic-type decays are found in glassy systems, where the dynamics takes place through activated processes. For example, recent studies have reported logarithmic relaxations in the orientational behaviour of supercooled molecular fluids[20] interpreted in the framework of the standard mode-coupling theory for glasses[21].

The slow activated relaxation involves topological rearrangement. After the system has reached its minimum in elastic energy, that is, for $t \approx (2\text{–}3) \times \tau_S$, DLs move only by virtue of thermal noises. These continued motions lead DLs to transiently adopt conformations less energetically favoured, and thus foster DL collisions that may result in topological changes, if more energetically favoured configurations (that is, with shorter DLs) can be accessed by the system after the collision. Such events can be directly visualized in the simulated RPM, as shown in Fig. 5, where we show two DL rearrangements taking place for $t \gg \tau_S$ in which the contact between two DLs has led to a change in their trajectories (see Supplementary Movies S1 and S2). A simple scaling analysis confirms that the free energy required for DL collision, which determines the activation barrier, scales proportionally to ℓ (see Supplementary Information). Indeed, if a porous structure is uniformly enlarged while keeping elastic constants and DL connectivity unchanged, the free energy required for bringing together two given DLs grows linearly with the expansion factor. Inspection of the simulations also provides us with a clue to understand the logarithmic nature of the relaxation. Each DL collision event leading to topological rearrangement is followed by a fast viscoelastic relaxation to a new state in which DLs experience a new energy landscape. This leads to a cascade effect, in which the activation energies are modified as the relaxation proceeds. Specifically, a logarithmic decay is generated if the activation energy grows with an inverse proportionality to $Q(t)$, that is, if the DL reorganization leads to increasingly high energy barriers for further DL collisions. This seems reasonable because DL reorganization yields progressively shorter DL loops that are further apart (see Supplementary Information).

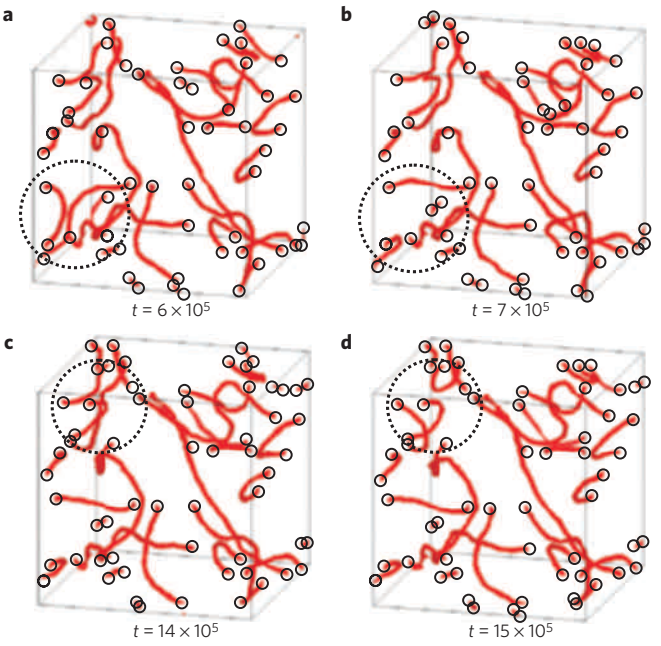

Figure 5 | Snapshots of defect lines (red lines) in RPM at selected times during their relaxation after removal of the field. a–d The comparisons between snapshots **a** and **b**, as well as between snapshots **c** and **d**, enable us to detect topological changes in the DLs of the NLC (see the locations marked by black dotted circles). Here the matrix is not shown. The end points of DLs on the surface of a simulation box are marked by black circles.

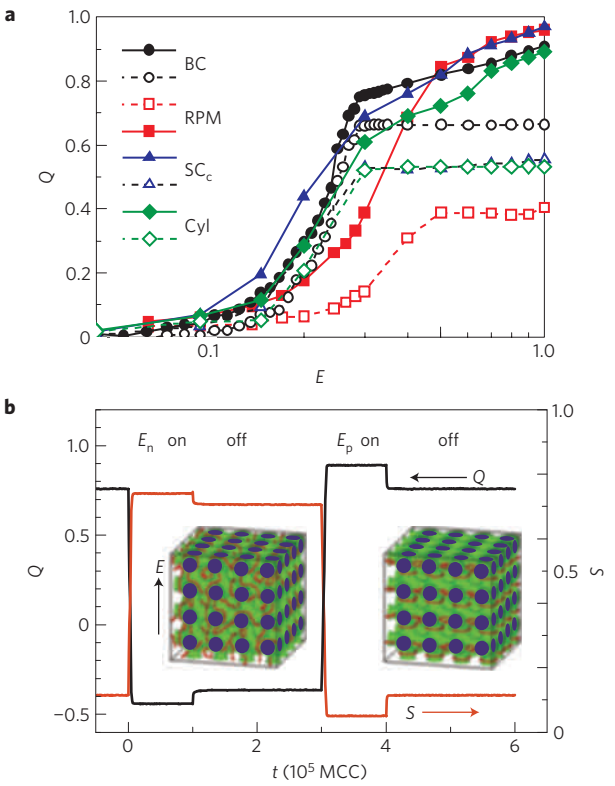

Figure 6 | Functionalization of NLC by confinements for memory applications. a, Field-strength dependence of the induced and remnant order for the various porous structures. Q_E (filled symbols) and Q_M (open symbols) are shown as functions of the field coupling strength E at $T = 0.1$. For RPM, Q_M represents the value for large ℓ (dashed blue line in Fig. 4b). The characteristic pore size of RPM is $\ell = 12.7$. Here BC, SC_c and Cyl ($L = 16$) are the same porous media as those in Fig. 1. **b**, Switching of dual-frequency NLC compounds confined in a BC structure ($L = 16$). An electric field with negative dielectric coupling ($\tilde{E} = 0.5$; $\Delta\epsilon < 0$) is applied in the interval $t = 0$–1×10^5 MCC, and an electric field with positive coupling ($\tilde{E} = 0.5$; $\Delta\epsilon > 0$) is applied in the interval $t = 3$–4×10^5 MCC. The approximate integrated scattering intensity S is also plotted (see also Supplementary Information). Snapshots of the defect structures after the two pulses are also shown.

In view of the higher memory found in the BC structure relative to the RPM, we examine the degree of remnant order in the other periodic porous media. This is shown in Fig. 6a, which summarizes the E dependence of Q_E and Q_M at $T = 0.1$ for the various systems. Q_E is found to be about the same in all ordered structures, with some differences in the threshold field. The remnant order, instead, is significantly different. The comparison between the various structures confirms the existence of a hierarchy of memorization capability $Q_M(BC) > Q_M(SC_c) \sim Q_M(Cyl) > Q_M(RPM)$. It should be noticed that RPM is the only system without NLC channels in the field direction, whereas SC_c, Cyl and BC share the same basic cubic symmetry, with one of the principal axes aligned with the field. The differences in their behaviours are to be sought in the coupling between surface curvature and DLs. The most efficient memorization is found in BC, where the geometry stabilizes small regular DL loops perpendicularly to the applied field. This stabilization, the origin of which was discussed above, combined with the fact that in this geometry the DL loops are small and well separated, contributes to minimizing topological restructuring due to DL collisions. Moreover, this structure produces the steepest E dependence of Q_E and Q_M, indicating that BC also provides the sharpest threshold for alignment transition. Finally, we note that we confirm the relevance of our simulation results to experiments for the case of RPM (see Supplementary Information).

'Geometrical functionalization' of NLC can be exploited to design devices able to memorize optical properties. This goal can be pursued with two main strategies (more detail in Supplementary Information): (1) polarization control devices, in which different metastable states yield different optical transmissions when the material is enclosed between crossed polarizers; (2) scattering control devices, in which different states are characterized by markedly different scattering cross-sections for light. In the first case, the large Q_M obtained with BC provides an effectively isotropic material for light propagating in the direction of E, and a highly birefringent material when the field is applied perpendicularly to the direction of propagation of light. The modulation of the scattering cross-section can instead be achieved in dual-frequency NLC compounds, the dielectric anisotropy of which changes sign with frequency[22]. Accordingly, the coupling with the electric field favours the alignment of the director along and perpendicularly to z at low and high frequencies, respectively. Hence, although positive dielectric anisotropy favours coherent orientation and hence suppresses fluctuations in the optical polarizability, negative polarization produces a strongly inhomogeneous and hence highly scattering state, where the director fluctuates within the x–y plane. The effect of the reversal of dielectric anisotropy and the resulting change in the approximate integrated scattering intensity S (see Methods) are shown in Fig. 6b, where electric pulses along the z-axis are applied between 0 and 10^5 MCC with negative dielectric coupling, and between 3×10^5 and 4×10^5 MCC with positive dielectric coupling. Quite clearly, negative dielectric coupling, favouring an orientation degenerate in the x–y plane, randomizes the defect structure. The state obtained in this way shows a very long lifetime, analogously to states previously described in BC.

The physical principle revealed here, being based on symmetry and topology, should be common to ferromagnetic

and superconducting materials. Recently, topologically stable objects such as skyrmions, hedgehogs or merons have received great theoretical and experimental interest in connection to the emergence of gauge theories in condensed matter. These objects may be considered as the building blocks of previously unknown forms of electronic order, as in the case of the skyrmion lattice in magnets[23], or in the case of organized vortex loops in mesoscopic superconductors[24]. The growing attention and increased capability in constructing nanostructured heterogeneous materials will certainly lead to investigating the interplay between the internal symmetry of these systems and the constraints arising from confinement. We see our work as a step towards topological functionalization of materials with complex order participating in heterogeneous structures.

Methods

Simulation methods. Lattice-based Monte Carlo simulations of confined NLCs were carried out by partitioning the simulated cubic lattice into three portions: $\mathcal{P}$ is the ensemble of lattice sites representing the solid material of the porous matrix; $\mathcal{N}$ denotes the nematic fraction described by headless spins $\mathbf{n}_i$ ($|\mathbf{n}|=1$) mutually interacting through the Lebwohl–Lasher potential[25,26]; $\mathcal{S}$ is the ensemble of spins lying at the interface with the solid fraction and thus interacting with it. Then the resulting Lebwohl–Lasher Hamiltonian is expressed as

$$\mathcal{H} = -\tilde{J}\sum_{\langle i,j\rangle\in\mathcal{N}\cup\mathcal{S}}(\mathbf{n}_i\cdot\mathbf{n}_j)^2 - \tilde{W}\sum_{i\in\mathcal{S}}(\mathbf{n}_i\cdot\mathbf{s})^2 - \mathrm{sign}(\Delta\epsilon)\tilde{E}^2\sum_{i\in N}(\mathbf{n}_i\cdot\mathbf{z})^2 \qquad (3)$$

The first term in the right-hand side represents the interaction between neighbouring spins belonging to $\mathcal{N}$ or $\mathcal{S}$. $\tilde{J}$ is the interaction strength and we set $\tilde{J}=1$ in all simulations. The second term describes the molecular anchoring to the surface of a porous matrix[27], $\mathbf{s}$ ($|\mathbf{s}|=1$) being the local surface normal and $\tilde{W}$ the anchoring strength. For positive $\tilde{W}$, the director tends to align normal to the surface ('homeotropic' anchoring). We set $\tilde{W}=1$ in all the simulations shown in this article. The third term accounts for the coupling of the NLC to the external field, the direction of which is along the z axis, and $\mathrm{sign}(x)$ is the sign function. Here, $\tilde{J}$, $\tilde{W}$ and $\tilde{E}$ are approximately given, respectively, by $\tilde{J}=Kd/2$, $\tilde{W}=Wd^2/2$, and $\tilde{E}^2=|\Delta\epsilon|E^2d^3/2$, where d is the lattice size, K is the elastic constant, W is the anchoring strength in the Rapini–Rapoular form, $\Delta\epsilon$ is the dielectric anisotropy of the NLC and E is the external electric-field strength. In this article, we express $\tilde{E}$ as E for simplicity.

We impose periodic boundary conditions. The simulation box was 128^3 cubic lattices for RPM, whereas $4L\times4L\times4L$ for BC, SC and Cyl, where L is the lattice constant of ordered structures. Each simulation result shown in Figs 2, 3, 4 and 6 was averaged over five runs. The average orientational order is calculated as $Q\equiv\langle Q^{zz}\rangle=(1/V_{\mathcal{N}})\sum_{i\in\mathcal{N}}Q_i^{zz}$, where $Q_i^{zz}=(3/2)(n_i^z n_i^z-1/3)$, n_i^z represents the z component of $\mathbf{n}_i$ and $V_{\mathcal{N}}$ is the number of $\mathcal{N}$ sites.

Details on Monte Carlo simulations. We employ heat-bath sampling for Monte Carlo simulations. A trial rotation of the ith spin is accepted, considering the local configurations of neighbouring spins, with the probability $p(\Delta\mathcal{H}_i)=1/(1+\mathrm{e}^{\Delta\mathcal{H}_i/T})$, where $\Delta\mathcal{H}$ is the difference of the Hamiltonian between before and after the trial rotation. The physical meaning of the temporal evolution of Monte Carlo simulations is sometimes a matter of debate. However, we note that the method has been known to be very powerful and useful for studying glassy systems with slow relaxations, such as a spin glass[28,29], the dynamics of which is dominated by activation processes overcoming a free-energy barrier.

Preparation of porous media with various geometries. We have considered various choices of $\mathcal{P}$, $\mathcal{N}$ and $\mathcal{S}$ within the class of bicontinuous geometries. To model the structure of the Millipore filters previously used in experiments[14], we have mimicked their production process. Accordingly, we have solved the Cahn–Hilliard–Cook equation for spinodal decomposition[30] on the cubic lattice and have let the system isotropically phase-separate into two phases, to be identified with $\mathcal{P}$ and $\mathcal{N}$. The volume fraction of the two phases is held to 50% by the initial condition. The resulting bicontinuous pattern grows self-similarly with time, thus enabling definition of a family of RPM structures differing in ℓ, defined as $\ell=2\pi/q_m$. q_m is the characteristic wavenumber of the structure factor of RPM, $S(\mathbf{q})$, and is given by $q_m=\int\mathrm{d}\mathbf{q}|\mathbf{q}|S(\mathbf{q})/\int\mathrm{d}\mathbf{q}S(\mathbf{q})$. In the left column of Fig. 1, an RPM for $\ell=12.0$ is shown by rendering the green solid matrix (blue inside). We use the same definition of ℓ for the other porous media.

Additionally, we simulated the behaviour of NLCs incorporated in three different symmetric and periodic porous matrices with symmetry axes aligned along E. Among them is the bicontinuous cubic (BC), one of the simplest ordered bicontinuous structures, expressed as $\cos(2\pi x/L)+\cos(2\pi y/L)+\cos(2\pi z/L)=0$, where L is its lattice constant. The characteristic length of porous media with different morphologies is also defined in the same manner as for RPM.

In each porous structure, we have annealed liquid crystals as shown in Fig. 2a for BC. We have first zero-field cooled ($E=0$) the nematic component through the isotropic–nematic transition (occurring at $T_{\mathrm{IN}}=0.749$) and let it equilibrate at the T of interest for 10^5 MCC. At $t_1=10^5$ MCC, we turn E on, and at $t_2=2\times10^5$ MCC we switch it off, letting the system further anneal at length, up to 10^7 MCC.

Estimation of the total integrated scattering intensity from NLC. We calculated the approximate integrated intensity of the scattering S from the director field by

$$S=\frac{1}{V}\sum_{i\in\mathcal{N},\mathcal{S},\mathcal{P}}\{(Q_{xx}{}^2-\langle Q_{xx}\rangle^2)+(Q_{yy}{}^2-\langle Q_{yy}\rangle^2)+2(Q_{xy}{}^2-\langle Q_{xy}\rangle^2)\} \qquad (4)$$

where $Q_{\alpha\beta}$ is the tensorial order parameter $Q_{\alpha\beta}=3/2(n_\alpha n_\beta-\delta_{\alpha\beta}/3)$, and $\langle X\rangle$ represents the spatial average of X. Here $Q_{\alpha\beta}$ is defined in the porous sites $\mathcal{P}$ because we set $\mathbf{n}_i=(0,0,1)$ for $i\in\mathcal{P}$. In equation (4), the summation is taken over all the lattice sites and V is the volume of the simulation box. We assume that the incident light propagates in the z direction and the scattering is induced by the inhomogeneities of n_x and n_y.

Received 18 May 2010; accepted 1 February 2011; published online 20 March 2011

References

1. Kleman, M. & Lavrentovich, O. D. *Soft Matter Physics: An Introduction* (Springer, 2003).
2. Crawford, G. P. & Žumer, S. (eds) *Liquid Crystals in Complex Geometries Formed by Polymer and Porous Networks* (Taylor and Francis, 1996).
3. Kim, J-H., Yoneya, M. & Yokoyama, H. Tristable nematic liquid-crystal device using micropatterned surface alignment. *Nature* **420,** 159–162 (2002).
4. Golemme, A., Žumer, S., Allender, D. A. & Doane, J. W. Continuous nematic–isotropic transition in submicron-size liquid-crystal droplets. *Phys. Rev. Lett.* **61,** 2937–2940 (1988).
5. Terentjev, E. M. Disclination loops, standing alone and around solid particles, in nematic liquid-crystals. *Phys. Rev. E* **51,** 1330–1337 (1995).
6. Poulin, P., Stark, H., Lubensky, T. C. & Weitz, D. A. Novel colloidal interactions in anisotropic fluids. *Science* **275,** 1770–1773 (1997).
7. Stark, H. Physics of colloidal dispersions in nematic liquid crystals. *Phys. Rep.* **351,** 387–474 (2001).
8. Bradač, Z., Kralj, S. & Žumer, S. Molecular dynamics study of nematic structures confined to a cylindrical cavity. *Phys. Rev. E* **58,** 7447–7454 (1998).
9. Araki, T. & Tanaka, H. Colloidal aggregation in a nematic liquid crystal: Topological arrest of particles by a single stroke disclination line. *Phys. Rev. Lett.* **97,** 127801 (2006).
10. Wu, X., Goldburg, W. I., Liu, M. X. & Xue, J. Z. Slow dynamics of isotropic–nematic phase transition in silica gels. *Phys. Rev. Lett.* **69,** 470–473 (1992).
11. Bellini, T. *et al.* Phase behavior of the liquid crystal 8CB in a silica aerogel. *Phys. Rev. Lett.* **69,** 788–791 (1992).
12. Iannacchione, G. S., Crawford, G. P., Žumer, S., Doane, J. W. & Finotello, D. Randomly constrained orientational order in porous glass. *Phys. Rev. Lett.* **71,** 2595–2598 (1993).
13. Bellini, T. *et al.* Nematics with quenched disorder: How long will it take to heal? *Phys. Rev. Lett.* **88,** 245506 (2002).
14. Buscaglia, M. *et al.* Memory effects in nematics with quenched disorder. *Phys. Rev. E* **74,** 011706 (2006).
15. Kang, D., Maclennan, J. E., Clark, N. A., Zakhidov, A. A. & Baughman, R. H. Electro-optic behavior of liquid-crystal-filled silica opal photonic crystals: Effect of liquid-crystal alignment. *Phys. Rev. Lett.* **86,** 4052–4055 (2001).
16. Radzihovsky, L. & Toner, J. Smectic liquid crystals in random environments. *Phys. Rev. B* **60,** 206–257 (1999).
17. Feldman, D. E. Quasi-long-range order in nematics confined in random porous media. *Phys. Rev. Lett.* **84,** 4886–4889 (2000).
18. Rutunno, M. *et al.* Nematics with quenched disorder: Pinning out the origin of memory. *Phys. Rev. Lett.* **94,** 097802 (2005).
19. Lammert, P. E., Rokhsar, D. S. & Toner, J. Topology and nematic ordering. I. A Gauge theory. *Phys. Rev. E* **52,** 1778–1800 (1995).
20. Cang, H., Novikov, V. N. & Fayer, M. D. Experimental observation of a nearly logarithmic decay of orientational correlation function in supercooled liquids on the picosecond-to-nanosecond time scales. *Phys. Rev. Lett.* **90,** 197401 (2003).
21. Götze, W. & Sperl, M. Nearly logarithmic decay of correlations in glass-forming liquids. *Phys. Rev. Lett.* **92,** 105701 (2004).
22. Yin, Y., Shiyanovskii, S. V., Golovin, A. B. & Lavrentovich, O. D. Dielectric torque and orientation dynamics of liquid crystals with dielectric dispersion. *Phys. Rev. Lett.* **95,** 087801 (2005).
23. Mühlbauer, S. *et al.* Skyrmion lattice in a chiral magnet. *Science* **323,** 915–919 (2009).

24. Doria, M. M., Romaguera, A. R. de C., Milosevic, M. V. & Peeters, F. M. Threefold onset of vortex loops in superconductors with a magnetic core. *Europhys. Lett.* **79,** 47006 (2007).
25. Lebwohl, P. A. & Lasher, G. Nematic-liquid-crystal order—Monte Carlo calculation. *Phys. Rev. A* **6,** 426–429 (1972).
26. Fabbri, U. & Zannoni, C. A Monte Carlo investigation of the Lebwohl–Lasher lattice model in the vicinity of its orientational phase transition. *Mol. Phys.* **58,** 763–788 (1986).
27. de Gennes, P. G. & Prost, J. *The Physics of Liquid Crystals* 2nd edn (Oxford Univ. Press, 1993).
28. Binder, K. & Kob, W. *Glassy Materials and Disordered Solids* (World Scientific Pub., 2005).
29. Ogielski, A. T. Dynamics of three-dimensional Ising spin-glasses in thermal equilibrium. *Phys. Rev. B* **32,** 7384–7398 (1985).
30. Onuki, A. *Phase Transition Dynamics* (Cambridge Unv. Press, 2002).

Acknowledgements

We thank C. P. Royall for a critical reading of the manuscript. This work was supported by a Grant in Aid from the Ministry of Education, Culture, Sports, Science, and Technology, Japan, and by the Cariplo Foundation (grant 2008-2413), Italy.

Author contributions

T.B. and H.T. conceived the project, T.A. carried out numerical simulations, M.B. carried out experiments and all authors analysed the data and wrote the manuscript.

Additional information

The authors declare no competing financial interests. Supplementary information accompanies this paper on www.nature.com/naturematerials. Reprints and permissions information is available online at http://npg.nature.com/reprintsandpermissions. Correspondence and requests for materials should be addressed to T.B. or H.T.